Mathematical Modeling of Electrode Cooling in Resistance Spot Welding

Mathematical models have been developed to simulate the electrode cooling in resistance spot welding and to evaluate a new cone-fin weld cap design capable of reducing the cap temperature

BY Z. H. RAO, S. M. LIAO, H. L. TSAI, P. C. WANG, AND R. STEVENSON

ABSTRACT

Due to the high heat flux from the weld nugget to the electrode, the electrode experiences thermal excursion and deformation, which lead to the requirement for frequent redressing or replacement of the weld cap. To extend the life of the weld cap, a better understanding of the thermal excursion experienced by the weld cap, and thus its cooling, is required. In this study, mathematical models that include the cooling water flow impinging onto the underside of the cap, resistance (or Joule) heating, as well as the heat transfer between the weld cap and the cooling water were developed. It was found that the conventional weld cap configuration results in a severe stagnation fluid flow near the underside of the weld cap and thus may lead to poor film boiling heat transfer there. Based on this understanding, a new cone-fin design on the underside of the weld cap was proposed to enhance the heat transfer. Our modeling results show that the fin not only lessens the stagnation flow near the cap but also increases the cooling area, leading to large reductions in temperatures at the underside of the weld cap. A roughened fin surface is also suggested to provide nucleation sites that can enhance the heat transfer between the cap and the cooling water due to nucleate boiling. Our implementation studies further confirm that the new cone-fin cap design can significantly extend the life of the weld cap.

Introduction

Resistance spot welding (RSW), as shown in Fig. 1, is the most widely used joining technique for the assembly of sheet metal components, especially in the automotive industry. It is characterized by high operating speeds and suitability for automation or robotization. During the process, sheet metal components are welded together as a result of the heat generated by electric resistance to current flow. The RSW process consists of first applying a force through the electrodes to clamp the workpieces and reduce the interface resistance and then passing a current through all the components shown in Fig. 1. As a result of the current flow, heat will be generated due to Joule heating. Since the welding current remains constant along the components, the location at which the greatest electrical resistance exists will generate the greatest heat. As the resistance of the interface between the two workpieces is dominant, a great deal of heat generated at the interface leads to an incremental rise in temperature of the weld cap. Therefore, owing to the effects of the mechanical force and electrical current, the weld cap is subjected to significant thermal and mechanical excursions. After a few welding cycles, the weld caps tend to be mushroomed resulting in the increase of the electrode tip area and thus the decreases of the holding pressure and current density (Ref. 1). Consequently, the current density will become smaller, which may not be high enough for effective welding. For this reason, the weld cap should be replaced or redressed, especially when welding thin workpieces. Hence, good cooling of the weld cap is essential in order to prevent it from becoming too hot and too soft. A number of experimental and modeling studies have attempted to address and better understand the aforementioned issue (Refs. 2–4). And much experimental research on electrode cooling water has been carried out to study the effects of water flow rate and water temperature (Refs. 5, 6). However, few detailed descriptions of modeling cooling water flow in the weld electrode and improving cooling efficiency during RSW have been reported.

In this study, we first focus our attention on developing a model for the fluid flow of cooling water in a "conventional" weld cap and, then, a time-dependent thermal model is developed to simulate the transient weld cap cooling process. Based on the fundamental understanding of the fluid flow and heat transfer characteristics for the conventional weld cap, a new cone-fin weld cap design is proposed and the corresponding mathematical model is developed aiming at the enhancement of the weld cap cooling. The new cap design is also implemented. Our modeling results show that in the new cap design the weld cap temperature is reduced, which is indirectly confirmed by our implementation studies in which the cap lifetime has been significantly extended.

KEYWORDS

Resistance Spot Welding
Electrode Cooling
Weld Cap
Transient Thermal Analysis

Mathematical Modeling

Figure 2A illustrates the geometry of the electrode including a conventional weld cap mounted on a supporting member (shank) with a cooling tube that pro-

Z. H. RAO is a PhD student and S. M. LIAO is a professor with the Central South University, Changsha, China. H. L. TSAI is a professor with the Missouri University of Science and Technology, Rolla, Mo. P. C. WANG and R. STEVENSON are technical fellows with GM R&D Center, Warren, Mich.

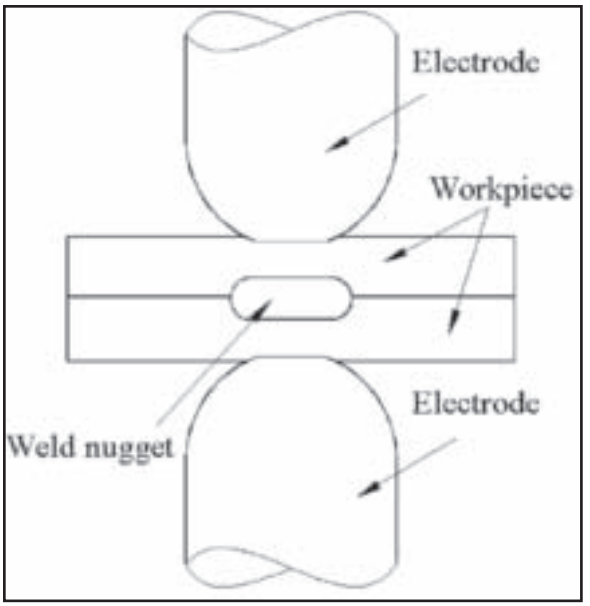

Fig. 1 — Schematic of the resistance spot welding process.

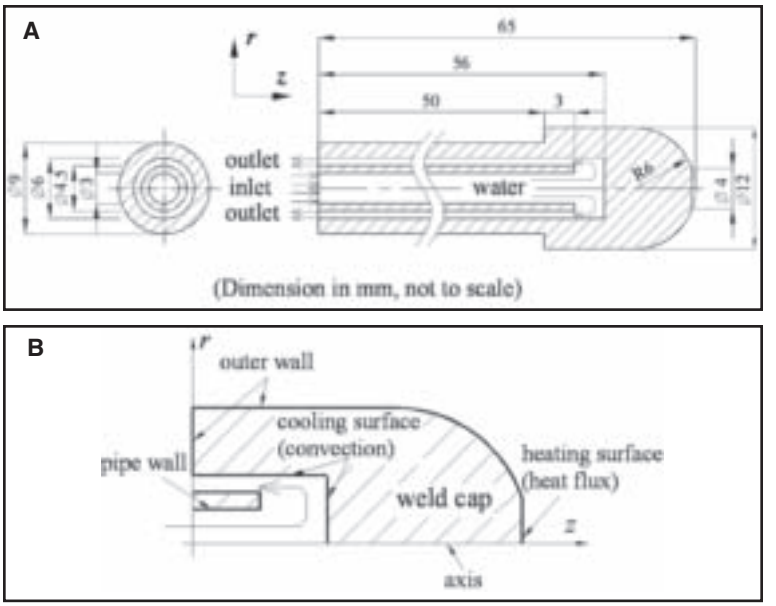

Fig. 2 — Schematic representation of the electrode with conventional weld cap: A — Geometry of the electrode; B — conventional weld cap and axisymmetrical computational domain.

vides cooling water. In this study, the shank-weld cap joint has been ignored, and the water supply tube is coaxially located relative to the shank wall. This simplification for modeling has negligible effects on the fluid flow in the cavity of the cap and the heat transfer between the cap and the cooling water compared to the actual setup (Ref. 7). The cooling water enters the cap cavity through the inner tube and leaves via the annular channel between the inner and the outer tubes.

Table 1 — Thermophysical Properties and Other Parameters

Nomenclature	Symbol	Value (unit)
Density of cap	ρ_c	8978 (kg/m^3)
Specific heat of cap	c_{pc}	381 (J/kg-K)
Thermal conductivity of cap	k_c	387.6 (W/m-K)
Electric conductivity of cap	σ_e	5.88×10^7 (Ω^{-1}m^{-1})
Density of cooling water	ρ_l	997.9 (kg/m^3)
Density of saturated water	ρ'	958.6 (kg/m^3)
Density of saturated steam	ρ''	0.596 (kg/m^3)
Density of superheated steam	ρ_v	0.565 (kg/m^3)
Specific heat of cooling water	c_{pl}	4176 (J/kg-K)
Specific heat of saturated water	c'_p	4214 (J/kg-K)
Specific heat of saturated steam	$c''p$	2075 (J/kg-K)
Specific heat of superheated steam	c_{pv}	2021 (J/kg-K)
Thermal conductivity of cooling water	k_l	0.608 (W/m-K)
Thermal conductivity of saturated water	k'	0.679 (W/m-K)
Thermal conductivity of saturated steam	k''	0.025 (W/m-K)
Thermal conductivity of superheated steam	k_v	0.0265 (W/m-K)
Viscosity of cooling water	μ_l	8.90×10^{-4} (kg/m-s)
Viscosity of saturated water	μ'	2.82×10^{-4} (kg/m-s)
Viscosity of saturated steam	μ''	1.23×10^{-5} (kg/m-s)
Viscosity of superheated steam	μ_v	1.30×10^{-5} (kg/m-s)
Surface tension of saturated water	σ	0.059 (N/m)
Latent heat of evaporation	h_{fg}	2.259×10^6 (J/kg)
Cooling water temperature	T_l	300 (K)
Saturated water temperature	T'	373.15 (K)
Multiplier in Equation 4	F	27.12
Multiplier in Equation 6	S	0.1
Local vapor volume fraction	α_{lh}	0.9

Modeling of Cooling Water Flow

The computational domain for modeling the cooling water flow is the cap cavity in the electrode that is idealized compared to real electrode caps, as shown in Fig. 2B. Due to symmetry arising from the presumed central location of the inlet flow tube, only one-half of the domain is considered. The inlet cooling water volume flow rate is assumed to be 2.46 L/min (0.65 gal/min) at 300 K, leading to about 5.8 m/s of average inlet velocity. The Reynolds number (*Re*) based on the tube diameter is about 17000 and, hence, the internal flow falls in the turbulent regime (Ref. 8). In the calculation, the relative pressure is used in the fluid flow field and a zero pressure is assumed at the outlet of the tube. The fluid flow governing differential equations based on the standard κ-ε turbulence model are solved using Fluent software (Ref. 9).

Figures 3A and B show, respectively, the calculated velocity vectors and pressure contours of the cooling water. As shown, the flow velocity decreases significantly near the center of the underside of the weld cap (at which the maximum temperature occurs), leading to a local high pressure region and a stagnation flow there. Hence, the cooling water may not be able to "sweep" the heat away from the weld cap. Previous experiments (Ref. 7) have demonstrated that the temperature

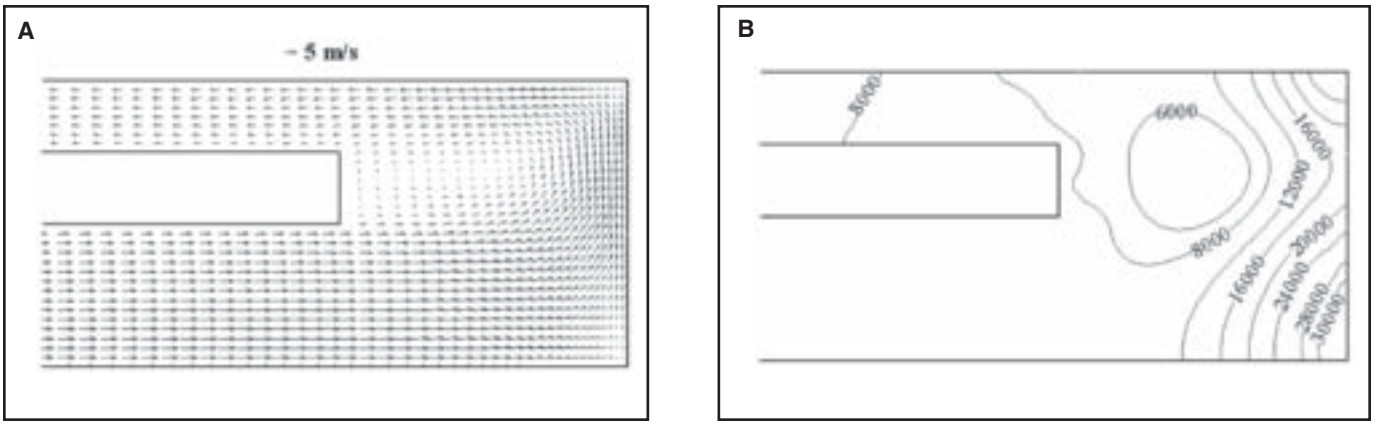

Fig. 3 — Calculated velocity vector and pressure contour for the cooling water in the conventional weld cap: A — Velocity vector; B — pressure contour (Pa).

at the underside of the weld cap can reach the boiling point of water. The very low flow velocity near the center of the weld cap will lead to an excessively high temperature of the weld cap, which may exceed the burnout point or the boiling crisis point (Ref. 10). As a result, the heat transfer mechanism between the cooling water and the weld cap may change from nucleate boiling to film boiling (Ref. 10). In the film boiling regime, the surface is blanketed by a film of vapor, and the heat transfer from the weld cap surface to the cooling water is by conduction across the vapor film, leading to a dramatic decrease of the heat transfer between the weld cap and cooling water. As a result, a further elevation of the cap temperature and thus a reduction in the strength of the cap will occur, which accelerates the softening and mushrooming of the cap.

Modeling of Weld Cap Temperature

Governing Equation

Figure 2B shows the computational domain of the weld cap in a cylindrical coordinate system that is enveloped by the heating surface, cooling surface, outer walls, and axis. For heat conduction in the axisymmetric weld cap, the governing equation is given by

$$\rho_c c_{pc} \frac{\partial T}{\partial t} = k_c \left(\frac{\partial^2 T}{\partial r^2} + \frac{1}{r}\frac{\partial T}{\partial r} + \frac{\partial^2 T}{\partial z^2} \right) + S \qquad (1)$$

where ρ_c is the density, c_{pc} is the specific heat, and k_c is the thermal conductivity of the cap. S is the source term from the bulk resistive heat generation by welding current (W/m^3).

Boundary Conditions

The boundary condition at the interior cooling surface is given by

$$-k_c \frac{\partial T}{\partial \vec{n}} = h\left(T_w - T_l\right) \qquad (2)$$

where $\vec{n}$ is the unit outer normal vector from the wall, T_w is the cap wall temperature, T_l is the cooling water temperature, and h is the convective heat transfer coefficient that depends on the flow characteristics of the cooling water. As discussed previously, boiling of the cooling water may occur at the inner surface of the cavity, which will lead to a complicated two-phase flow. Depending upon the characteristics of fluid flow and heat transfer, the heat transfer coefficient h in Equation 2 can be a combination of forced convection boiling h_1 and natural convection film boiling h_2, which are discussed below.

For forced convection boiling, the following convective heat transfer coefficient is considered to be the combination of single-phase liquid heat transfer and nucleate boiling heat transfer (Refs. 11, 12)

$$h_1 = h_c + h_{NB}\left(\frac{T_w - T'}{T_w - T_l}\right) \qquad (3)$$

where T' is the saturated water temperature and h_c corresponds to the single-phase liquid heat transfer and is obtained from the following Dittus-Boelter equation modified by a multiplier F

$$h_c = 0.023\frac{k_l}{d} F \times Re_l^{0.8} Pr_l^{0.4} \qquad (4)$$

where the subscription l is for liquid, Pr is the Prandtl number, and F is determined by the Martinelli factor (Ref. 11). The nucleate boiling heat transfer coefficient h_{NB}, proposed by Forster and Zuber (Ref. 13), is employed in this study and given by

$$h_{NB} = c\left(p'\left[\min\left(T_w, 647\right)\right] - p_0\right)^{0.75} \left(T_w - T'\right)^{0.24} \qquad (5)$$

where

$$c = 0.00122 S \left(\frac{k' c_p'}{\sigma}\right)^{1/2} \mathrm{Pr}_l^{-0.29} \rho'^{1/4} \left(\frac{c_p' \rho'}{\rho'' h_{fg}}\right)^{0.24} \qquad (6)$$

where the superscript "prime" refers to the saturated water, the "double prime" superscript refers to vapor phase, p_0 is atmospheric pressure, σ is the surface tension, and h_{fg} is the latent heat of evaporation. The multiplier S, defined as the ratio of the effective superheat to the total superheat of the wall, is a function of the Reynolds number provided by Bjornard and Grifith (Ref. 14).

The heat transfer coefficient for film boiling in this study is given by

$$h_2 = h_{FB}\left(\frac{T_w - T'}{T_w - T_l}\right) \qquad (7)$$

where h_{FB} is the film boiling heat transfer coefficient. For natural convection film boiling on a horizontal plane, Berenson (Ref. 15) proposed the following expression

$$h_{Berenson} = 0.425\left(\frac{k_v^3 \rho_v \left(\rho' - \rho''\right) h_{fg} g}{\mu''\left(T_w - T'\right)\lambda_{RT}}\right)^{1/4} \qquad (8)$$

where

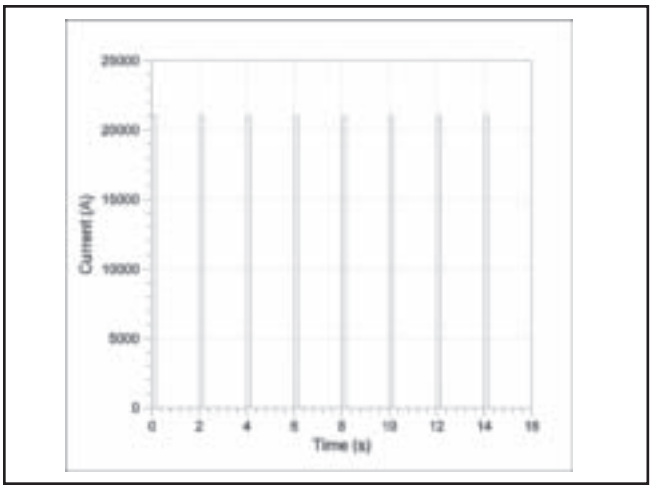

Fig. 4 — Weld current vs. time for a typical resistance weld.

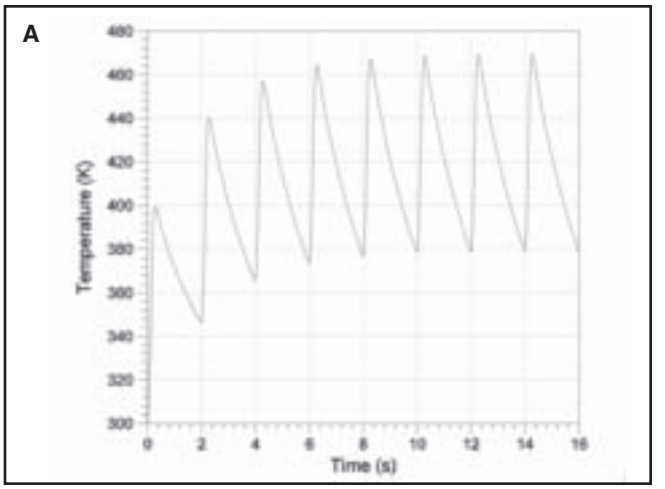

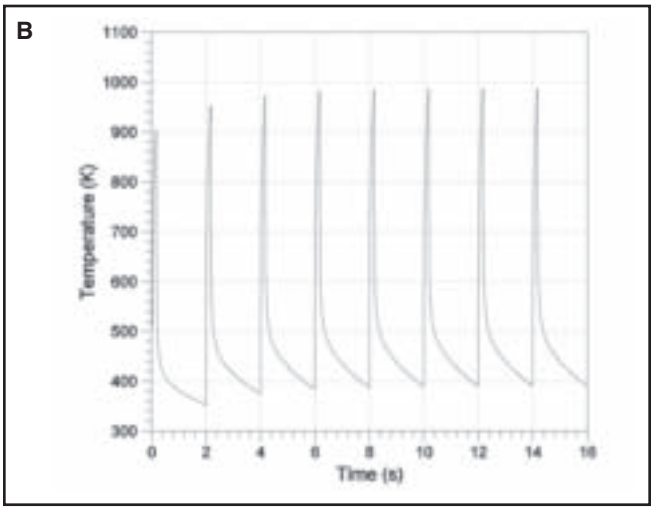

Fig. 5 — Calculated transient temperature at the underside center (z = 6 mm, r = 0 mm) and at the tip (z = 14.66 mm, r = 0 mm) of the weld cap: A — At the underside center; B — at the tip.

$$\lambda_{RT} = \left[\frac{\sigma}{g(\rho' - \rho'')}\right]^{1/2} \qquad (9)$$

where the subscript v is for vapor and g is the gravitational acceleration. For natural convection film boiling in channel with very low mass flux, Leperriere (Ref. 16) modified the Berenson's equation to obtain a correlation as

$$h_{FB} = h_{Berenson}\left(1 + 25.5\frac{T_w - T'}{T_l}\right)$$

$$(1-\alpha_{1h})^{0.5} \qquad (10)$$

where α_{1h} is the local vapor volume fraction (Ref. 16).

Based on the calculated flow characteristics and above discussion, the heat transfer mechanism along the cooling surfaces may involve several different regimes, including single-phase liquid heat transfer, nucleate boiling, and film boiling. Therefore, the heat transfer coefficient h in Equation 1 is regarded to be a weighted average of heat transfer coefficients h_1 and h_2, which can be expressed as

$$h = \alpha_1 h_1 + (1-\alpha_1)h_2 \qquad (11)$$

where α_1 corresponds to the ratio of forced convection boiling heat flux to the total heat flux. Strictly speaking, the heat transfer coefficient h can be time and location dependent, and depends on the fluid flow and heat transfer characteristics. In this study, we assume $\alpha_1 = 0.5$, an average of the forced convection boiling and the natural convection film boiling. Note a constant temperature T_l of 300 K is assumed for cooling water, which is reasonable because the high flow rate results in only a few degrees (K) of temperature increase for fluid core through the cavity (Ref. 1). As a result, the heat transfer in the internal fluid core is ignored. For heat conduction in the weld cap, various cooling rates due to the various heat transfer coefficients between the walls and cooling water are considered by Equations 2–11. It is also noted that the wall temperature T_w and the heat transfer coefficient h are coupled, and iterations are required in the calculation.

The boundary condition at the heating surface (see Fig. 2B) is considered as Joule heating flux due to contact resistance at the interface between the weld cap and workpiece. The contact resistance consists of the constriction resistance and the resistance from possible surface contamination. In general, contact resistance may vary both spatially and temporally. In this study, the contact resistance is assumed to be constant, and half of the power input determined by the experiment (Ref. 4), 910 W, is used, yielding a heat flux of $q = 7.24 \times 10^7$ W/m^2. For the outer walls (see Fig. 2B), the heat loss may consist of both the natural convection and thermal radiation. However, in this study the natural convection and radiation heat loss are negligible as compared to the convective heat transfer to the cooling water. Hence, the boundary condition at the outer walls is simply set as an adiabatic condition ($q = 0$).

Generation of Joule Heat

The bulk Joule heat generation due to electric resistance is determined by Ohm's law. Hence, the source term in Equation 1 can be derived as

$$S = \frac{J^2}{\sigma_e} = \sigma_e E^2 \qquad (12)$$

where σ_e is the electric conductivity of the material, J is the electric current density, and E is the magnitude of the electric field. In order to obtain the electric field, the following Poisson's equation must be solved.

$$\frac{1}{r}\frac{\partial}{\partial r}\left(\sigma_e r\frac{\partial \phi}{\partial r}\right) + \frac{\partial}{\partial z}\left(\sigma_e \frac{\partial \phi}{\partial z}\right) = 0 \qquad (13)$$

where ϕ is the electric potential, and the two components of the electrical field can be found via

$$E_r = -\sigma_e \frac{\partial \phi}{\partial r};\ E_z = -\sigma_e \frac{\partial \phi}{\partial z} \qquad (14)$$

Finally, the magnitude of the electric field E

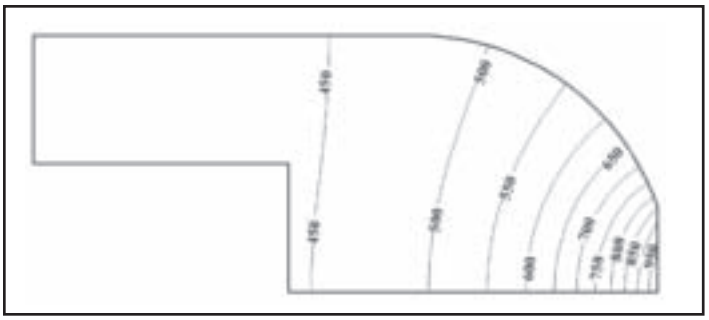

Fig. 6 — Temperature contour (K) of the conventional weld cap at a weld time of 14.165 s.

is computed, which is the square root of E_r^2 and E_z^2.

Numerical Procedure

Equations 1 and 13, subjected to all required boundary conditions, are solved implicitly with a time step size of 0.005 s. At each time step, Equations 3–10 are first solved based on a new wall temperature to obtain the heat transfer coefficient through Equation 11. The boundary condition at the interior cooling surface is then updated using Equation 2. Equations 13 and 14 are also solved to obtain the new electric field and update the source term *S* using Equation 12. And then Equation 1 is solved to obtain a new distribution of temperature in the weld cap. Next, the calculation goes back to the first step. This process is repeated for each time step until the convergence criteria for wall temperature are satisfied.

Results and Discussion

In this study, the welding system is stationary and the time-dependent welding process with the given welding current cycles is shown in Fig. 4. In each cycle (2 s), an electric current of 21 kA is applied during the first 0.165 s and then is shut off for 1.835 s (Ref. 4). Thus, the heat flux at the heating surface and the bulk resistive heat source are generated periodically. Note some real welding current features are not considered in this study. The effect of multiple weld cycles (representative of the thermal exposure experienced by the weld cap when multiple sequential welds are made robotically in an individual station) is investigated by repeating this cycle eight times corresponding to eight welds made at 2-s intervals (i.e., robot duty cycle is 8). The thermophysical properties of the weld cap (copper) and water (Ref. 17) are listed in Table 1 with other parameters used for the calculation.

Transient Temperatures

Figure 5A and B show, respectively, the transient temperature at the underside center (z = 6 mm, r = 0 mm) and the tip (z = 14.66 mm, r = 0 mm) of the weld cap. As shown in the figures, both the temperatures at the underside center and the tip of the weld cap increase rapidly after the cessation of electric current, as expected. The peak temperatures of the cap tip and the underside of the weld cap are about 985 and 470 K, respectively. The tip temperature decays rapidly after the electric current is ceased, while the temperature at the underside decreases slowly. The tip temperature remains "steady" after about four welding cycles, but it takes about six welding cycles for the underside of the cap. The predicted temperature trends for the cap underside are generally in good agreement with the experimental measurements (Ref. 7) where water boiling was observed. Figure 6 shows the temperature contour in the weld cap at t = 14.165 s for the last welding cycle.

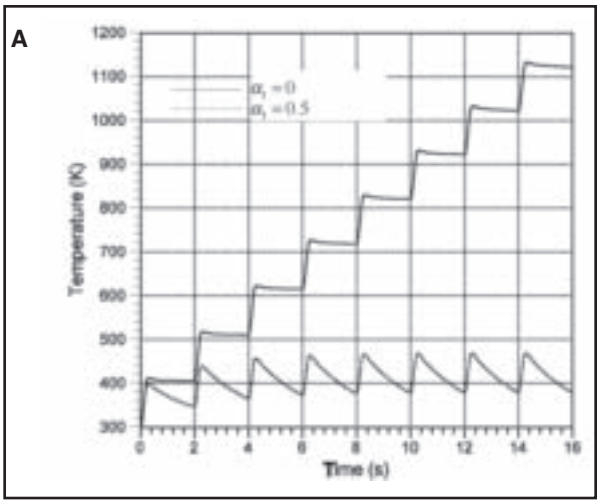

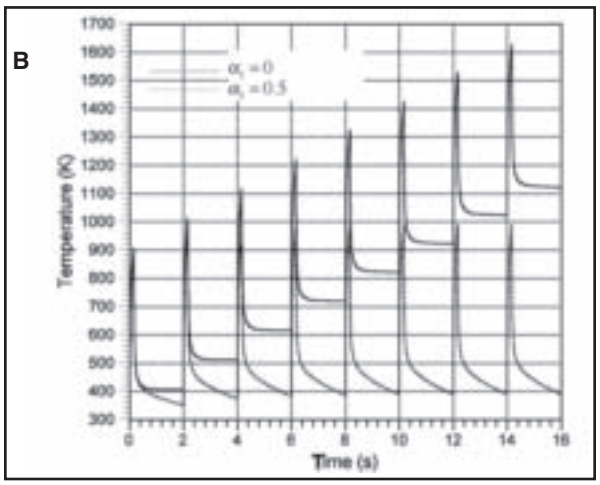

Fig. 7 — Effect of convective heat transfer coefficient on the transient temperature at the underside center (z = 6 mm, r = 0 mm) and at the tip (z = 14.66 mm, r = 0 mm) of the weld cap: A — At the underside center; B — at the tip.

As shown in Fig. 5B, under repeated weld cycles, the transient behavior associated with each individual weld cycle is superimposed on an increasing background temperature that quickly approaches an asymptotic limit (steady state) after several welding cycles, especially for the electrode with the high thermal conductivity. At the asymptotic limit, the heat loss to the cooling water balances with the heat input and generation during one cycle. Hence, the temperature varies periodically in a repeated fashion and no further increase in peak temperature takes place. Thus, the thermally driven mechanism of cap degradation will not be further enhanced even if more welds are added to a robot duty cycle. However, there is approximately 85 K difference in peak temperature between the first and the eighth weld cycle, which plays a significant role in accelerating the weld cap degradation. Thus, while an increase in the number of welds in a duty cycle will not significantly increase the rate of cap degradation provided the background temperature has achieved its asymptotic limit, a decrease in the number of welds in the duty cycle, which enables a reduction in the background temperature, will effectively reduce the rate of weld cap degradation, and extend the weld cap life.

The above calculated results indicate that the underside wall temperature of the weld cap falls in the range of 300–500 K. As a result, the heat transfer coefficient h is in the order of 10^4 W/m^2–K that is about the average of film boiling and nucleate boiling. Hence, our assumption of using α_1 = 0.5 appears to be reasonable. However, it would be worthwhile to study the effects of the heat transfer coefficient on temperature cycles of the weld tip and the underside. Figure 7A and B, respectively, shows the transient temperature profiles at the underside center and the tip of the

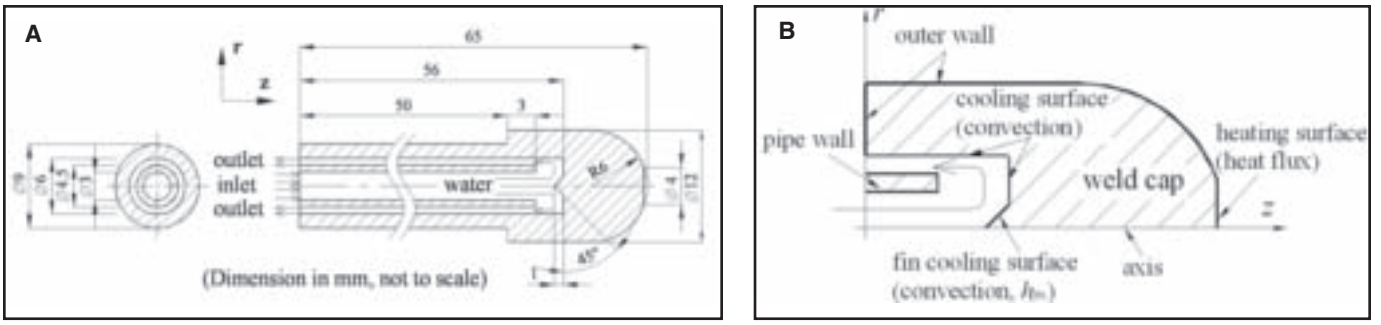

Fig. 8 — A schematic representation of the electrode with new weld cap design: A — Geometry of the electrode; B — new weld cap design and axisymmetrical computational domain.

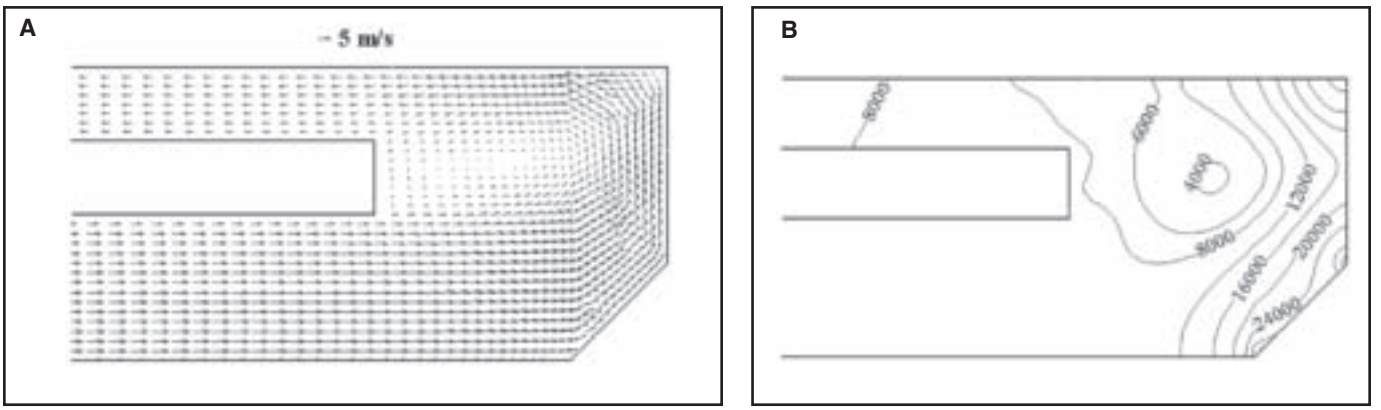

Fig. 9 — Calculated velocity vector and pressure contour for the cooling water in the new weld cap: A — Velocity vector; B — pressure contour (Pa).

weld cap between the cases with $\alpha_1 = 0$ and $\alpha_1 = 0.5$ (the case shown in Fig. 5). When $\alpha_1 = 0$, the heat transfer coefficient is calculated by Equation 7 and in the order of 10^2 W/m^2–K, which corresponds to the formation of a vapor film around the inner surface of the cap as a result of the stagnation flow of the cooling water. With the low heat transfer coefficient, our modeling results show that the quasi-steady state would never be achieved. This suggests that for each weld cycle the heat input is always larger than the heat removal and, consequently, the peak temperature increases progressively and promotes ever-increasing weld cap degradation. Note that, as shown in Fig. 7A, B, the differences in corresponding temperatures between the two cases are not significant during the first welding cycle. This is because the response from the cooling water is slow compared to the short welding duration of 0.165 s. Note similar results were also found by Yeung and Thornton (Ref. 4) that the convective heat transfer coefficient has little effect on the peak temperature for the first welding cycle. However, after the following cooling cycles the weld cap temperature cannot be restored to its initial condition as $\alpha_1 = 0$, indicating both the background temperature and the peak temperature increase continuously.

New Weld Caps

The calculated velocity vectors and pressure contours are shown in Fig. 9A and B, respectively. It can be seen that near the underside of the weld cap, stagnation flow has been significantly reduced. The cooling water sweeps and carries away the heat transferred from the weld tip. Hence, the new cap design can effectively lessen the stagnation of the flow and avoid the occurrence of film boiling near the center of the cooling surface. Since boiling of cooling water near the cap underside is still inevitable, maintaining the nucleate boiling might be a good way to improve the heat transfer by taking advantage of large latent heat of vaporization. This can be achieved by roughening the surface of the cone-fin. The roughened surface would provide many nucleation sites for boiling, thereby suppressing film boiling and dramatically augmenting the heat transfer.

Figure 8B shows the calculation domain for modeling the new weld cap with a cone-fin of a height of 1 mm and a base radius of 1 mm, which is enveloped by the heating surface, cooling surface, outer walls, fin, and axis. In this model, most conditions are the same as the conventional design without a fin, but a higher convective heat transfer coefficient in the fin area is used. Based on the above discussion, as there is no stagnation flow near the cone-fin and a possible nucleate boiling, the value of α_1 in Equation 11 is higher. For simplification, two constant heat transfer coefficients for the fin h_{fin} are assumed in the modeling (i.e., 30,000 and 50,000 W/m^2–K), which are in the range of the results obtained from Equation 3 for the forced convection boiling heat transfer. Note the selected values of the convective heat transfer coefficients are typical for nucleate boiling. It is also noted the heat transfer coefficient for the other cooling surface is coupled with wall temperature and, hence, iterations are required using the aforementioned method. Figure 10A, B show, respectively, the transient temperatures at the underside center ($z = 6$ mm, $r = 0$ mm) and the tip ($z = 14.66$ mm, $r = 0$ mm) of the new weld cap. It is seen that, compared to the case without a cone-fin, the temperatures at the underside of the weld cap are significantly decreased. The temperature reductions at the underside of the weld cap for a heat

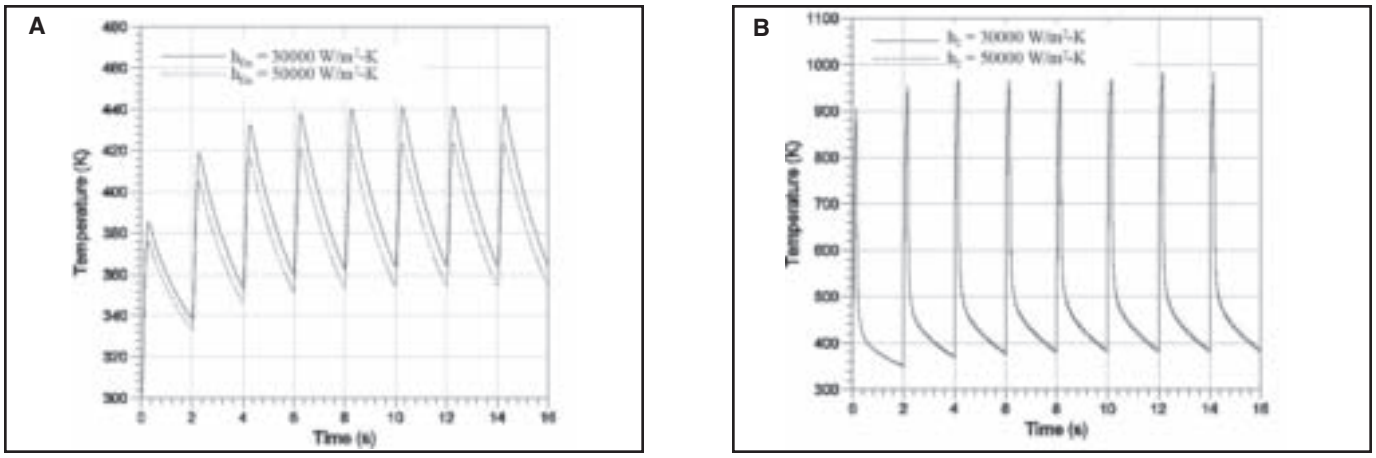

Fig. 10 — Effect of heat transfer coefficients of the fin on the transient temperature at the underside center (z = 6 mm, r = 0 mm) and at the tip (z = 14.66 mm, r = 0 mm) of the weld cap (h_{fin} = 30,000 W/m²–K or 50,000 W/m²–K): A — At the underside center; B — at the tip.

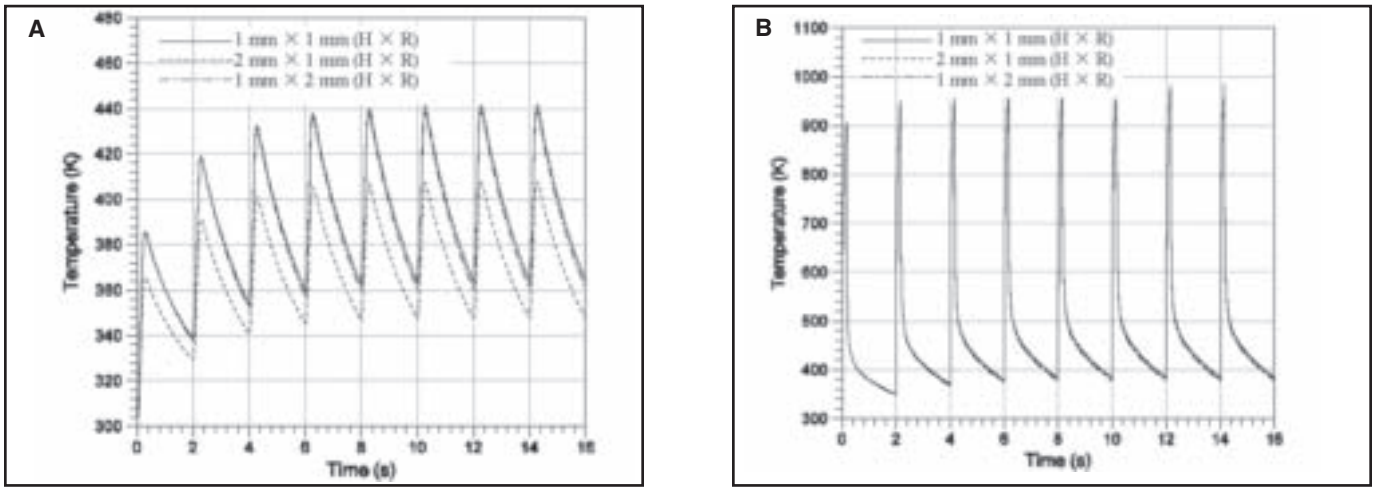

Fig. 11 — Effect of fin geometry on the transient temperature at the underside center (z = 6 mm, r = 0 mm) and at the tip (z = 14.66 mm, r = 0 mm) of the weld cap (H = height, R = base radius): A — At the underside center; B — at the tip.

transfer coefficient h_{fin} of 30,000 W/m²–K and 50,000 W/m²–K are 30 and 50 K, respectively. However, the temperature at the tip of the weld cap is determined by the heat dissipation rate from the tip and heat flux onto the tip. The heat flux for each case is unchanged due to the same welding current profile and contact resistance. As shown in Fig. 10B, when a cone fin is added, the temperature at the tip only has a slight decrease at the end of each cycle due to the slow response from heat removal by cooling water compared to the welding cycle duration (2 s).

Effect of Fin Geometry

The above results indicate the addition of a cone-fin at the underside of the weld cap improves the heat transfer significantly. To optimize the fin geometry, in addition to the original fin geometry, two more fin geometries were studied; one fin-geometry has a height (H) of 2 mm and a base radius (R) of 1 mm, and the other has a height (H) of 1 mm and a radius (R) of 2 mm. The heat transfer coefficient for the fin is assumed to be 30,000 W/m²–K in both cases. Figure 11A, B show, respectively, the effects of fin geometry on the temperatures of the underside center and the tip of the weld cap. In comparison to the original fin with 1 mm height and 1 mm base radius, the fin with higher height (2 mm) further reduces the temperature at the underside center by about 30 K, while there is no obvious decrease in temperature for the case with greater radius (2 mm). This can attribute to the fin efficiency discussed below. However, for all these cases, the temperature differences at the tip are insignificant due to the reason discussed in Fig. 10B. These results suggest that the variation in fin geometry has little influence on the temperature of the cap tip.

A theoretical study of a cone-fin, with a constant base temperature, yields the following equation for the fin tip temperature (Ref. 18):

$$\frac{T_0 - T_\infty}{T_B - T_\infty} = \frac{m\sqrt{H}}{I_1\left(2m\sqrt{H}\right)} \qquad (15)$$

where T_0 is the temperature of the cone-fin tip, T_B is the temperature of the cone-fin base, T_∞ is the fluid flow temperature, I_1 is the modified first-order Bessel function of the first kind, and

$$m^2 = \frac{2h}{k}\sqrt{\left(\frac{H}{R}\right)^2 + 1}. \qquad (16)$$

The fin efficiency is defined as the ratio of the heat transfer rate for the case with a fin to the case without a fin. For an ideal cone-fin, its efficiency is given by

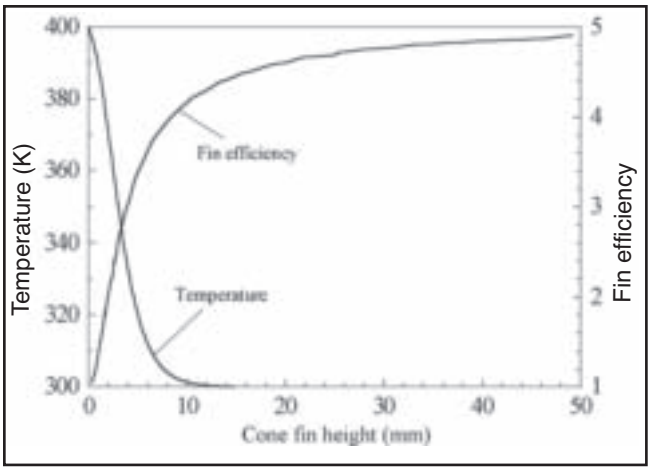

Fig. 12 — Effects of fin height on the fin tip temperature and the fin efficiency (h = 30,000 W/m²–K, k = 387.6 W/m–K, T_B = 400 K, T_∞ = 300 K, fin base radius R = 0.001 m).

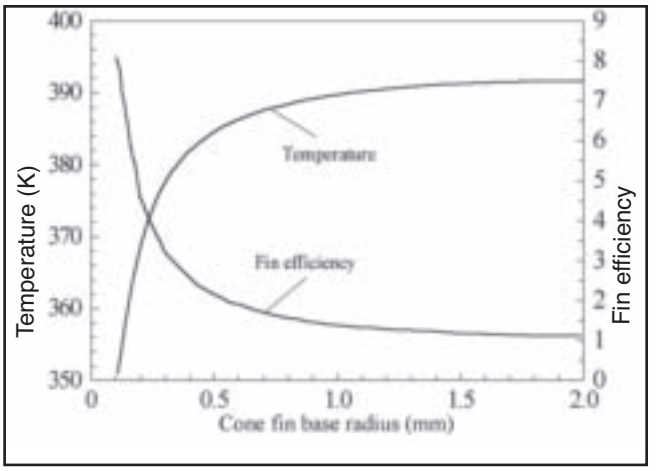

Fig. 13 — Effects of fin base radius on the fin tip temperature and the fin efficiency (h = 30,000 W/m²–K, k = 387.6 W/m–K, T_B = 400 K, T_∞ = 300 K, fin height H = 0.001m).

$$E = \frac{k}{hH}\left(m\sqrt{H}\,\frac{I_0\left(2m\sqrt{H}\right)}{I_1\left(2m\sqrt{H}\right)} - 1 \right) \qquad (17)$$

Figures 12 and 13 show, respectively, the variations of fin tip temperature and fin efficiency with respect to the variations of fin height and fin base radius. A convection heat transfer coefficient h = 30,000 W/m²–K and a thermal conductivity k = 387.6 W/m–K for the fin are used in the calculations. The cone-fin base temperature and fluid flow temperature are taken at 400 and 300 K, respectively. Thus, trends for the effects of the fin geometry parameters on local temperature obtained from the theoretical solution agree with our modeling results as discussed above. It appears a fin of larger height has a better efficiency. However, when the fin height exceeds a certain range, the heat transfer enhancement is no longer significant.

Implementation Studies

During the normal welding process, the tip area of the weld cap will grow by mushrooming and consequently the current density and pressure will decrease. To maintain the effective RSW process and weld quality, a schedule of electrode redressing should be set up. With other variables held constant, 60-Hz, single-phase AC at different levels was used to examine the aforementioned weld caps. The cap material used was Class II Cr-Cu alloy with a 4-mm tip diameter. It is assumed that the electrode should be redressed as the diameter of the electrode tip increases to 1.3 times the starting diameter (Ref. 1). Thus, the weld numbers of the electrode before its redressing were obtained. Extensive experiments have been conducted and only one representative result is presented here. As shown in Fig. 14, it can be seen that the new cone-fin design increases the weld number significantly. At the same current level, the weld number for the new cone-fin cap is much larger than that for a conventional weld cap. For both kinds of weld caps, the weld numbers increase with welding current in a nearly linear relationship. This is because the weld time and hold time can be shortened for each welding cycle at a higher current level. Although the temperatures of the underside and the tip of the weld cap were not measured for direct comparison with modeling predictions, apparently the new cone-fin design and our modeling predictions are generally correct for improving the weld cap cooling and extending the life of the weld cap.

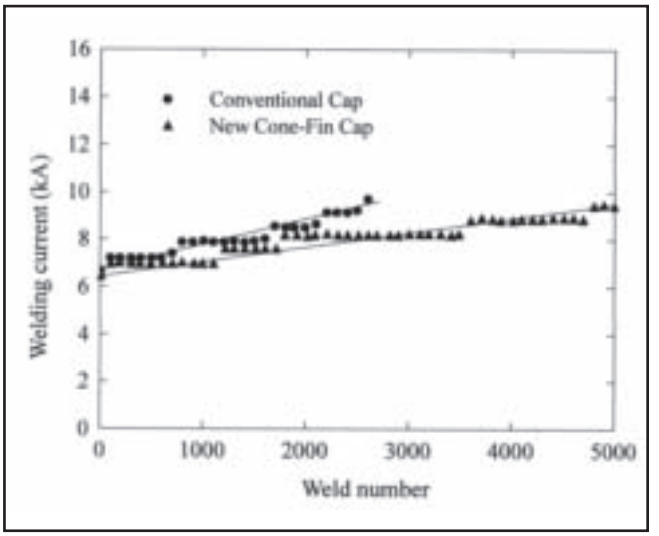

Fig. 14 — Weld number vs. welding current of different weld caps.

Conclusions

In this paper, models that include cooling water flow impinging onto the underside of the cap, heat generated by resistance to the flow of electric current in the weld cap, as well as heat transfer between the weld cap and the cooling water were developed. It was found that the conventional configuration of the weld cap results in stagnation of the fluid flow, leading to poor film boiling heat transfer at the underside of the weld cap. A new cone-fin design at the underside of the weld cap was proposed to enhance the heat transfer. The fin effectively suppresses the film boiling and thus reduces the risk of reaching the burnout temperature. A roughened fin surface is also suggested to provide nucleation sites that can enhance the heat transfer between the cap and the cooling water due to nucleate boiling. As a result, the new cone-fin reduces the temperature at the underside of the weld cap, enables the tip temperature to quickly approach an asymptotic limit, and prevents the mushrooming of the weld cap. The implementation studies confirm that the new cone-fin design can extend the life of the weld cap significantly. The mathematical modeling provides an invaluable guidance in the design of the weld cap for the RSW process.

Nomenclature

c_p	specific heat at constant pressure, J/kg–K
d	tube diameter, m
E	magnitude of the electric field, V/m
F	multiplier in Equation 4
g	gravitational acceleration, m/s^2
H	height of fin, m
h	effective heat transfer coefficient, W/m^2–K
h_{FB}	film boiling heat transfer coefficient, W/m^2–K
h_c	convective heat transfer coefficient, W/m^2–K
h_{NB}	nucleate boiling heat transfer coefficient, W/m^2–K
h_{fg}	latent heat of evaporation, J/kg
I	electric current, A
I_0, I_1	Bessel functions
J	electric current density, A/m^2
k	thermal conductivity, W/m–K
n	unit outer normal vector from the wall
p	pressure, Pa
Pr	Prandtl number
q	heat flux, W/m^2
r–z	cylindrical coordinate system
R	base radius of fin, m
Re	Reynolds number
S	source term in Equation 1, or multiplier in Equation 6
T	temperature, K

Greek

α_1	ratio of forced convection boiling heat flux to the total heat flux
α_{1h}	local vapor volume fraction
μ	dynamic viscosity of liquid, kg/m-s
ϕ	electric potential, V
σ	surface tension, N/m
σ_e	electric conductivity, Ω^{-1}m^{-1}
ρ	density, kg/m^3

Superscript and Subscript

'	saturated liquid
"	saturated steam
l	liquid
v	gas
w	wall
c	cap

References

1. Williams, N. T. 1993. Resistance spot welding. *ASM Handbook*, Vol. 6: Welding, Brazing and Soldering. ASM International, Materials Park, Ohio. p. 226,

2. Browne, D. J., Chandler, H. W., Evans, J. T., and Wen, J. 1995. Computer simulation of resistance spot welding in aluminum: Part I. *Welding Journal* 74(10): 339-s to 344-s.

3. Feng, Z., Bau, S. S., Santella, M. L., Reimer, B. W., and Gould, J. E. 1998. An incrementally coupled electrical-thermal-mechanical model for resistance spot welding. 5th International Conference on Trends in Welding Research, Pine Mountain, Ga.

4. Yeung, K. S., and Thornton, P. H. 1999. Transient thermal analysis of spot welding electrodes. *Welding Journal* 78(1): 1-s to 6-s.

5. Kim, E., and Eagar, T. W. 1998. Transient thermal behavior in resistance spot welding. *Proceedings, Sheet Metal Welding Conference 2* (AWS-Detroit Section, Southfield, Mich.). Oct. Paper 2.

6. Hirsch, R. 1996. Influence of water temperature and flow on electrode life. *Proceedings, Sheet Metal Welding Conference 7* (AWS-Detroit Section, Troy, Mich.). Oct. Paper E3.

7. Karagoulis, M., Private communication, General Motors Corp.

8. Shames, I. H. 1992. *Mechanics of Fluids*, McGraw-Hill.

9. 2004 FLUENT software, ANSYS, Inc., Canonsburg, Pa.

10. Tong, L. S., and Tang, Y. S. 1997. *Boiling Heat Transfer and Two-Phase Flow*, Taylor & Francis.

11. Chen, J. C. 1963. A correlation for film boiling heat transfer to saturated fluids in convective flow. ASME Publication-63-HT-34: 2–6.

12. Groeneveld, D. C., Chen, S. C., Leung, L. K. H., and Nguyen, C. 1989. Computation of single and two phase heat transfer rates suitable for water-cooled tubes and subchannels. *Nuclear Engineering and Design*, 114: 61–77.

13. Forster, H. K., and Zuber, N. 1955. Dynamic of the vapor bubbles and boiling heat transfer. *AIChE Journal*, 1(4): 531–535.

14. Bjornard, T. A., and Grifith, P. 1977. PWR blow-down heat transfer, Thermal and Hydraulic Aspects of Nuclear Reactor Safety, American Society of Mechanical Engineers, New York, Vol. 1: 17–41.

15. Berenson, P. J. 1961. Film boiling heat transfer from a horizontal surface. *J. Heat Transfer* 83(3):351-358.

16. Leperriere, A. 1983. An analytical and experimental investigation of forced convective film boiling, M.A. Sc. thesis, University of Ottawa, Ottawa, Canada.

17. Harvey, A. H., Peskin A.P., and Klein S.A. 2004. NIST/ASME Steam Properties Database. National Institute of Standards and Technology.

18. Incropera, F. P., Dewitt, D. P. 2001. *Fundamentals of Heat and Mass Transfer*, 5th Edition, John Wiley and Sons, New York.

CAN WE TALK?

The *Welding Journal* staff encourages an exchange of ideas with you, our readers. If you'd like to ask a question, share an idea or voice an opinion, you can call, write, e-mail or fax. Staff e-mail addresses are listed below, along with a guide to help you interact with the right person.

Publisher
Andrew Cullison
cullison@aws.org, Extension 249
Article Submissions

Editor
Mary Ruth Johnsen
mjohnsen@aws.org, Extension 238
Feature Articles

Associate Editor
Howard Woodward
woodward@aws.org, Extension 244
Society News
Personnel

Associate Editor
Kristin Campbell
kcampbell@aws.org, Extension 257
New Products
News of the Industry

Production Manager
Zaida Chavez
zaida@aws.org, Extension 265
Design and Production

Advertising Sales Director
Rob Saltzstein
salty@aws.org, Extension 243
Advertising Sales

Advertising Sales & Promotion Coordinator
Lea Garrigan Badwy
garrigan@aws.org, Extension 220
Production and Promotion

Advertising Production Manager
Frank Wilson
fwilson@aws.org, Extension 465
Advertising Production

Peer Review Coordinator
Erin Adams
eadams@aws.org, Extension 275
Peer Review of Research Papers

Welding Journal Dept.
550 N.W. LeJeune Rd.
Miami, FL 33126
(800) 443-9353
FAX (305) 443-7404

WELDING journal

Guidelines for submitting electronic files

1. Platform:
Macintosh or PC accepted

2. Files accepted:
QuarkXpress, Adobe Photoshop, Adobe Illustrator, TIFF, EPS and PDF files only.

3. Color:
Send all files in as CMYK (for color) or Grayscale (for b/w).

4. Images:
Minimum resolution required for magazine printing is 300 dpi for full color artwork or grayscale at least 1000 dpi for bitmap (B&W/line art). Images and logos from Web sites are NOT usable for printing. They are low resolution images (72 dpi). Images taken with a digital camera are not acceptable unless they meet the minimum 300 dpi requirement.

5. Proof:
A proof of the images should **always** be provided.

6. Electronic File Transfer:
Files larger than 20 MB are not acceptable as an email attachment; please send it on a CD or Zip, you may also send files to the printer FTP site (a user name and password will be provided when requested)

Check list for submitting electronic files:

Colors: ❒ 4/C ❒ Grayscale ❒ B&W/line art

File Type: ❒ TIFF ❒ EPS

File sent via: ❒ DVD ❒ Zip disk ❒ CD ❒ Email

❒ **Proof supplied**/faxed

❒ CMYK images at 300 dpi or higher, B&W/line art at 1000 dpi or higher.

❒ All color in all images set to CMYK process (not RGB)

When submitting ads, please send them to the attention of

Frank Wilson
Advertising Production Manager
American Welding Society
550 NW LeJeune Rd.
Miami, Fla. 33126